OPEN ACCESS
JOURNAL OF ADVANCED DIELECTRICS
Vol. 12, No. 6 (2022) 2241004 (8 pages)

DOI: 10.1142/S2010135X22410041

Influence of the prestressed layer on spherical transducer in sound radiation performance

Xiaofang Zhang*, Xiujuan Lin*, Rui Guo*, Changhong Yang*,‡, Hui Zhao†,§, Mingyu Zhang†, Yan Wang†, Xin Cheng* and Shifeng Huang*,¶

*Shandong Provincial Key Laboratory of Preparation and Measurement of Building Materials
University of Jinan, 336 Nanxinzhuang West Road, Jinan, Shandong 250022, P. R. China

†Underwater Acoustic Transducer Lab, Shanghai Marine Electronic Equipment Research Institute
Shanghai 201108, P. R. China

‡mse_yangch@ujn.edu.cn

§zhaohui0094@163.com

¶huangshifeng_ujn@163.com

Received 14 August 2022; Revised 6 October 2022; Accepted 16 October 2022; Published 24 November 2022

To improve the acoustic radiation performance of the spherical transducer, a prestressed layer is formed in the transducer through fiber winding. The influence of the prestressed layer on the transducer is studied from the effects of the radial prestress (T_r) and acoustic impedance, respectively. First, a theoretical estimation of T_r is established with a thin shell approximation of the prestressed layer. Then, the acoustic impedance is measured to evaluate the efficiency of sound energy transmission within the prestressed layer. Further, the ideal effects of T_r on the sound radiation performances of the transducer are analyzed through finite element analysis (FEA). Finally, four spherical transducers are fabricated and tested to investigate their dependence of actual properties on the prestressed layer. The results show that with the growth of T_r, the acoustic impedance of the prestressed layer grows, mitigating the enormous impedance mismatch between the piezoelectric ceramic and water, while increasing attenuation of the acoustic energy, resulting in a peak value of the maximum transmitting voltage response (TVR_{max}) at 1.18 MPa. The maximum drive voltage increases with T_r, leading to a steady growth of the maximum transmitting sound level (SL_{max}), with a noticeable ascend of 3.9 dB at a 3.44 MPa T_r. This is a strong credibility that the prestressed layer could improve the sound radiation performance of the spherical transducer.

Keywords: Radial prestress; acoustic impedance; spherical transducers; transmission voltage response; transmission sound level.

1. Introduction

Piezoelectric materials show unique features to convert electrical energy into mechanical energy and vice versa.[1] Researches have been working to improve the properties of the piezoelectric materials,[2–4] considering its usage in transducers,[5,6] resonators,[7,8] energy harvesters[9] and other devices. Among the various applications, the piezoelectric transducers show excellent performances, including small size, low cost, and good stability.[10,11] With the development of underwater detection, the demand for the transducer with wide-angle detection capability becomes more and more urgent. However, many piezoelectric transducers exhibit near-field directionality,[12,13] which generates and receives acoustic waves along limited directions, resulting in complex sensor networks or transducer arrays to realize full area coverage.[14] Hence, the spherical piezoelectric transducer, which could offer true three-dimensional omnidirectional capability in all frequencies,[15] is deemed a suitable omnidirectional sound emission source.[16]

Furthermore, with the increasing requirements for the high power transmission transducers, how to further improve the acoustic radiation performance of transducers based on existing technology has become a research hot spot in the academic field. It is found that the vibration mode for an omnidirectional spherical piezoelectric transducer is the radial mode.[17] Equations have established the relationships between strains, displacements, and electrical potentials in hollow piezoceramic spheres with radial polarization.[18] Usually, when the spherical piezoelectric transducers act as transmitting probes, they are excited by high voltages. The resulting large strains may reach the mechanical stress limits in the piezoelectric ceramics.[19] In other words, although a high voltage is conducive to improving the acoustic output of the transducer,[20,21] it increases the risk of ceramic fracture and transducer damage with the low tensile limit of the piezoelectric ceramics.[22] An effective solution to avoid this risk is to introduce prestress.[23,24]

Researchers have found that mechanical prestress is one of the primary factors which affect the transducer's

¶Corresponding author.

performance.[25,26] The piezoelectric charge coefficient and the permittivity change drastically when the ceramic undergoes high uniaxial stress.[27,28] When the mechanical prestress is lower than 50 MPa, changes in the effective contact surface between transducer parts cause shifts in resonance and anti-resonance frequencies of piezoelectric transducers.[29] The prestress could even suppress the spurious resonance and increase the vibration velocity of the transducer.[30] Up to now, there are three main methods to control prestress for transducers. First, for transducers with prestressed bolts, it is convenient to control the prestress quantitatively with a gauged torque wrench or a simple electronic circuit.[31,32] Adjustable prestress was further designed for flextensional transducer with rotational and rectilinear motions of the transition block.[33] Second, the metal thin circular ring with high thermal conductivity is adopted to apply radial pre-stressing on the surface of the piezoelectric tubes.[34,35] Third, fiber winding is used to apply radial prestress on the outer surface of the piezoelectric ceramic tubes.[36] Overall, it is difficult to use a bolt or a metal shell to realize uniform and quantitative prestress on the surface of the hollow piezoceramic sphere which is curved in three-dimensional. Combined with the successful cases of fiber winding for the spherical pressure vessels,[37] it is practical to form a prestressed layer on the outer radius of the hollow piezoelectric spheres.

Herein, geodesic filament winding is adopted to realize various radial stresses and form prestressed layers on the surface of the hollow piezoelectric spheres. A theoretical estimation of the radial stress is established with a thin shell approximation, and the acoustic impedance of the prestressed layer is measured. Then, the effects of radial prestress and voltage on the performances of the piezoelectric ceramic are analyzed with finite element analysis (FEA), including the resonance frequency (f_r), the transmission voltage response (TVR), and the transmitting sound level (SL). Finally, four spherical transducers are manufactured and tested in an anechoic pond to verify their sound radiation performances. This work could help the design and application of prestressed spherical transducers.

2. Experimental Methods

2.1. *Geodesic filament winding*

The geodesic filament winding strategy is adopted to realize various radial prestresses on the surface of the hollow piezoelectric spheres (PZT 4, Yu Hai Electronic Ceramics Co., Ltd., China). The multi-axis winding equipment (JNW01-50, Hunan Jiangnan Machinery (Group) Co. LTD, China) controls the tensile force of the glass fiber (1080TEX, width 4.0 mm, thickness 0.2 mm) and the number of the fiber layers. Figure 1 illustrates the process of the geodesic filament winding strategy and an example of a prestressed composite sphere. During the geodesic filament winding, the sphere was fixed through the two holes on its tops. The glass

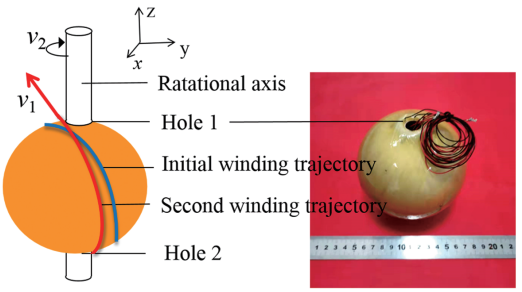

Fig. 1. The process of the geodesic filament winding and the prestressed hollow piezoelectric sphere.

fiber was soaked in epoxy resin composite (Model 3601, Shanghai Huayi Resin Co., Ltd, China) with a mass ratio of 0.445:0.555 for epoxy and curing agent. The epoxy was cured in 6 h at 80°C.

2.2. *Spherical transducers*

Four spherical transducers numbered from 1# to 4# were fabricated to study the actual underwater sound radiation performances. 1# transducer was a standard spherical transducer without prestressed layer, and 2#–4# were prestressed transducers with various prestessed layers. The structures of the standard and prestressed spherical transducers were almost the same except that the prestressed layer of the standard transducer was replaced by the sealing layer, as presented in Fig. 2.

The metal rod to clamp the hollow piezoelectric sphere was 304 steel. The sealing material was polyurethane (RC0801, Shanxi Chemical Research Institute, China), cured for 8 h at 80°C in an oven (Model Gl-2001, Shandong Longkou Xianke Instrument Co., LTD).

2.3. *Characterization*

2.3.1. *Characterization of the prestressed layer*

To research the properties of the prestressed layer, three prestressed layers with various thicknesses of fiber were made. The density and thickness of the prestressed layer were

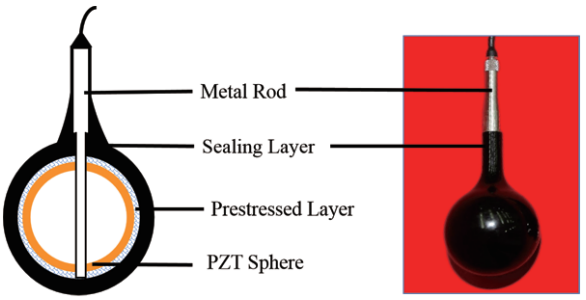

Fig. 2. Structure of the spherical transducer.

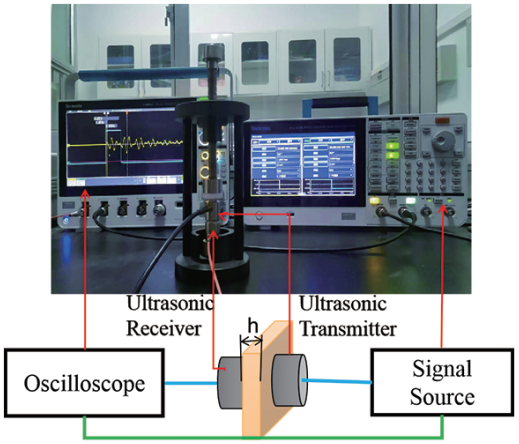

Fig. 3. Setup of the estimation of acoustic impedance.

measured through a helical micrometer and an electronic density meter (Model DK-300A, Xiamen Eisite Co., LTD., China), respectively. With the assistance of a signal source (Model AFG 31000, Teck Technology (China) Co., LTD, China), an oscilloscope (Model MDO 3000, Teck Technology (China) Co., LTD, China) and two ultrasonic transducers (Model R15α, Physical Acoustics Corp., USA), the time delay of the acoustic wave passing through the prestressed layer was measured, and then the acoustic impedance could be estimated, as shown in Fig. 3.

2.3.2. *Characterization of the transducer*

The resonance frequency (f_r) of the spherical transducers was measured by the impedance analyzer (Model 4900A, Key sight Technologies Co. Ltd., America). The TVR and the transmitting sound level (SL) were measured at an anechoic pond (China Shipbuilding Industry Corp 726, China).

3. Results and Discussion

3.1. *Characterization of the prestressed layer*

The prestressed layer applies radial prestress on the outer surface of the hollow piezoelectric sphere. The radial stress is estimated theoretically with the connection of the fiber winding parameters. Meanwhile, the acoustic impedance of the prestressed layer is evaluated.

3.1.1. *Radial prestress estimation*

A theoretical estimation of the radial stress is performed with a thin shell approximation of the prestressed layer because the thickness of the prestressed layer (approximately 1–2 mm) is much less than the average radius (about 46 mm). According to the theory of elasticity, the stress components of the spherical shell under internal and external pressure are[38,39]:

$$T_r = P_0 \frac{r_0^3\left(r^3 - r_i^3\right)}{r^3\left(r_i^3 - r_0^3\right)} - P_i \frac{r_i^3\left(r_0^3 - r^3\right)}{r^3\left(r_i^3 - r_0^3\right)}, \tag{1}$$

$$T_\theta = T_\varphi = P_0 \frac{r_0^3\left(2r^3 + r_i^3\right)}{2r^3\left(r_i^3 - r_0^3\right)} - P_i \frac{r_i^3\left(2r^3 + r_0^3\right)}{2r^3\left(r_i^3 - r_0^3\right)}, \tag{2}$$

where T_r is the radial stress component of the hollow spherical shell, T_θ and T_φ are the tangential stress components; P_i and P_o are the internal and external pressures; r_i and r_o are the inner and outer radii of the spherical shell, r is the radius at which the stress is evaluated. The prestressed layer is formed as a sphere outside the hollow piezoelectric sphere with a static pressure which is assumed as P, as shown in Fig. 4.

The boundary conditions of the prestress sphere are $r = R_2$, $P_i = P$; $r = R_3$, $P_o = 0$. Hence, the stress components of the prestressed layer could be expressed and simplified from Eqs. (1) and (2) as:

$$T_{rf} = -P \frac{R_2^3\left(R_3^3 - r_f^3\right)}{r_f^3\left(R_2^3 - R_3^3\right)}. \tag{3}$$

$$T_{\theta f} = T_{\varphi f} = -P \frac{R_2^3\left(2r_f^3 + R_3^3\right)}{2r_f^3\left(R_2^3 - R_3^3\right)}. \tag{4}$$

where the index f indicates the prestress sphere, R_2 and R_3 are the inner and outer radii of the prestress sphere, r_f is the radius of the prestress sphere at which the stress is evaluated. According to the generalized Hooke law, the relationship between the tensile force (F) controlled in the geodesic filament winding and the stress (T_f) distribution in the prestressed fiber layer could be expressed as:

$$T_f = \frac{F}{wt}, \tag{5}$$

where w and t are the width and thickness of the fiber.

The decomposition of stress $T(r, \theta, \varphi)$ is performed along r, θ, and φ in the spherical coordinate system, as shown in Fig. 5.

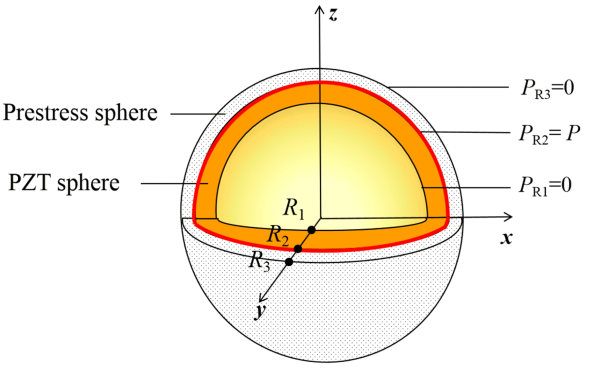

Fig. 4. Stress analysis of the prestressed sphere.

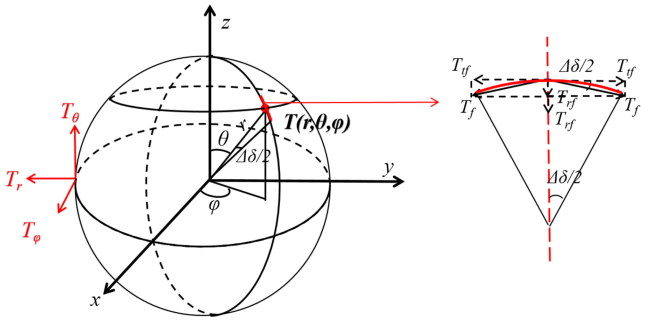

Fig. 5. Stress analysis on an element of the prestressed sphere.

If the radian of the fiber segment is small enough, the stress components could be further approximated as

$$T_{rf} = 2T_f \sin\left(\frac{\Delta\delta}{2}\right) \approx T_f \Delta\delta, \tag{6}$$

$$T_{tf} = T_f \cos\left(\frac{\Delta\delta}{2}\right) \approx T_f, \tag{7}$$

where T_{rf} and T_{tf} are the radial and tangential stress components, $\Delta\delta$ is the radian of the fiber segment. T_{tf} is further decomposed along the horizontal and vertical direction in the surface which is perpendicular to the radius as

$$T_{tf} = \sqrt{T_{\theta f}^2 + T_{\varphi f}^2}. \tag{8}$$

The combination of Eqs. (4), (5), (7), and (8) yields

$$P = -\frac{\sqrt{2}F}{wt} \frac{r_f^3\left(R_2^3 - R_3^3\right)}{R_2^3\left(2r_f^3 + R_3^3\right)}. \tag{9}$$

The substitution of Eq. (9) into Eq. (3) generates the radial stress at the interface of the ceramic and prestressed sphere as

$$T_r = \frac{\sqrt{2}F}{wt} \frac{R_3^3 - R_2^3}{2R_2^3 + R_3^3}. \tag{10}$$

Compared with the inner radius of the prestressed sphere (45 mm), the thickness of the fiber (0.2 mm) is quite small, and the value of radial stress generated by each fiber layer is approximated to be the same as Eq. (10). Thus, the total radial stress is rewritten as

$$T_r = -\frac{\sqrt{2}nF}{wt} \frac{R_3^3 - R_2^3}{2R_2^3 + R_3^3}, \tag{11}$$

where the outer radius is expressed as $R_3 = R_2 + t$, R_2 is the outer radius of the hollow piezoelectric spheres. It is noteworthy that the radial stress increases linearly with the number of fiber layers (n) and the tensile force (F), respectively. The radial stresses introduced in the prestressed spheres are listed in Table 1.

Table 1. Summary of the radial prestresses in the spherical transducers.

No.	F (N)	N	T_r(MPa)
1#	0	0	0
2#	75	2	1.18
3#	73	4	2.29
4#	73	6	3.44

3.1.2. *Acoustic impedance*

In order to get the maximum transmitted energy, the acoustic impedance of the acoustically transparent layer should be optimized. According to the theory of single matching layer, the optimal acoustic impedance (Z_t) between the piezoelectric ceramic (Z_c) and water (Z_w) is[40]

$$Z_t = \sqrt[3]{Z_c Z_w^2}. \tag{12}$$

In this paper, the typical values of Z_c and Z_w are calculated as 31.5 Mrayls and 1.5 Mrayls, respectively, and Z_t is 4.29 Mrayls.

The acoustic impedance of the prestressed layer is measured to evaluate the efficiency of sound energy transmission within the prestressed layer. The acoustic impedance of the prestressed layer could be calculated as[41]

$$Z_p = \rho\upsilon = \rho h_p/\Delta t, \tag{13}$$

where Z_p, ρ, υ and h_p are the acoustic impedance, density, acoustic velocity, and thickness of the prestressed layer, respectively; Δt is the time delay.

As listed in Table 2, the acoustic impedance (Z_p) of the prestressed layer grows with the number of the fiber (n), gradually approaching the optimal value. This variation indicates that Z_p would help mitigate the enormous impedance mismatch between the piezoelectric ceramic and water, reducing the reverberation of waves within the transducer.[42] Hence, more acoustic energy could pass the prestressed layer, bringing benefits for the acoustic performance of the transducer.

3.2. *Characterization of spherical transducers*

The ideal effects of the radial prestress on the performances of the transducer were analyzed through FEA. Four spherical transducers were fabricated and tested to verify the dependence of the actual transmitting properties on radial prestress.

Table 2. Summary of the properties of the prestressed layer.

n	ρ (kg/m^3)	h_p (mm)	Δt (μs)	υ (m/s)	Z_p (Mrayls)
2	1691	0.57	0.3	1831.1	3.1
4	1713	1.102	0.5	2185.2	3.7
6	1715	1.578	0.7	2279.0	3.9

Table 3. Summary of the material properties in FEA.

Mater	ρ (kg/m^3)	v (m/s)	ε_r	cE (10^{10}Pa)	eES (C/m^2)
Water	1000	1500	/	/	/
PZT 4	7500	/	{762.5, 762.5, 663.2}	{13.8999, 7.78366, 13.8999, 7.42836, 7.42836, 11.5412, 0, 0, 0, 0, 2.5641, 0, 0, 0, 0, 0, 2.5641, 0, 0, 0, 0, 0, 3.0581}	{0, 0, –5.20279, 0, 0, –5.20279, 0, 0, 15.0804, 0, 12.7179, 0, 12.7179, 0, 0, 0, 0}

3.2.1. *FEA prediction*

With the assistance of the FEA method, the ideal effect of radial prestress (T_r) on the acoustic performances of the spherical transducer is researched. We ignore the supporting structure, the sealing layer, and the hole across the piezoelectric ceramic to simplify the calculation. The material properties are listed in Table 3.

Considering the symmetry in the spherical geometry, only one-eighth of the sphere is remained in the three-dimensional model, with symmetry nodes to realize structural integrity.[16] As shown in Fig. 6, a boundary load is applied on the outer radius of the PZT sphere to describe the radial prestress. A linearly perturbed voltage excitation across the piezoelectric ceramic is applied. Besides, the constraints also include far-field calculation and perfectly matched layer (PML). Free tetrahedral mesh is used for PZT and water domain, and swept node is used for the PML layer, with eight layers to ensure adequate wave resolution. A stationary study is used to calculate the prestress distribution in the transducer, followed by a frequency domain perturbation to calculate the sound radiation performance of the transducer with an alternating current excitation. We varied the radial prestress (T_r) and the drive voltage (V_{rms}).

The dependence of the sound radiation performance on radial prestress and voltage is shown in Fig. 7. The resonance frequency (f_s) is defined as the frequency corresponding to the maximum conductance (G), and f_s remains relatively stable at 19.4 kHz with T_r.

The transmitting voltage response (TVR) is calculated as

$$\mathrm{TVR} = 20\log\left(\frac{P_f}{V_{\mathrm{rms}}}\right)+120, \tag{14}$$

where P_f is the acoustic pressure, V_{rms} is the effective drive voltage. TVR reaches the maximum transmitting voltage response ($\mathrm{TVR}_{\mathrm{max}}$) at 19.4 kHz. $\mathrm{TVR}_{\mathrm{max}}$ shows a minimal upward trend with T_r.

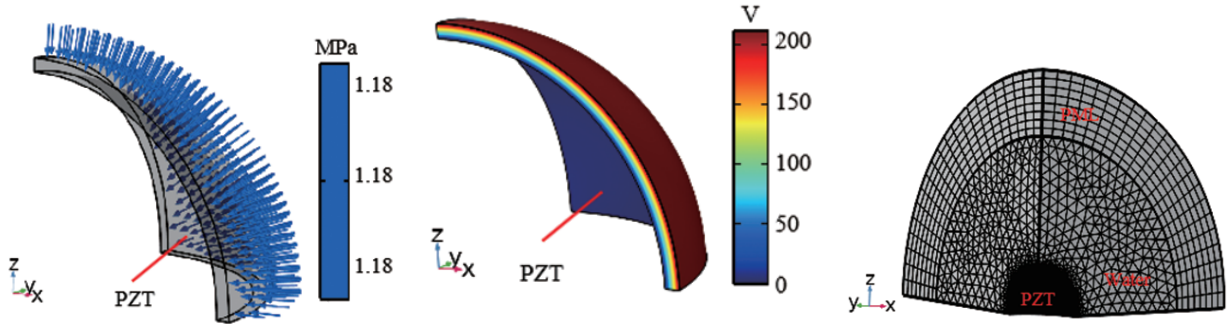

(a) (b) (c)

Fig. 6. Summary of the constrains of the spherical transducer model in FEA, (a) radial prestress, (b) voltage distribution, (c) meshed geometry.

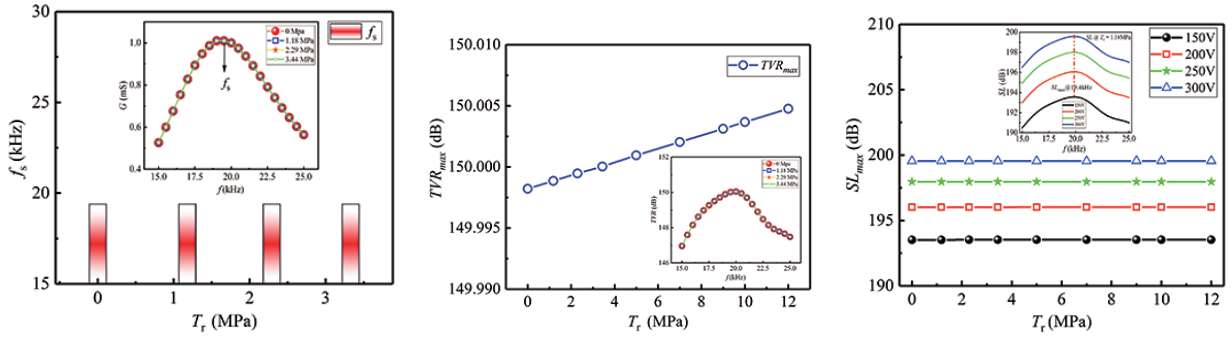

(a) (b) (c)

Fig. 7. Summary of FEA results of the spherical transducer in water, variation of (a) resonance frequency (f_s), (b) transmitting voltage response (TVR), and (c) transmitting sound level (SL) with radial prestress and voltage.

The transmitting sound level (SL) is calculated as

$$\mathrm{SL} = 20\log\left(V_{\mathrm{rms}}\right) + \mathrm{TVR}. \tag{15}$$

SL peaks at 19.4 kHz with various voltages and prestresses. Similar to $\mathrm{TVR}_{\mathrm{max}}$, the maximum transmitting sound level ($\mathrm{SL}_{\mathrm{max}}$) shows marginal growth with T_r. By contrast, $\mathrm{SL}_{\mathrm{max}}$ jumps markedly with voltage, from 193.5 dB at 150 V to 199.5 dB at 300 V. The noticeable growth of $\mathrm{SL}_{\mathrm{max}}$ forecasts that it is practical to improve the transmitting performance of the transducer by increasing the driving voltage.

3.2.2. *Experimental verification*

To investigate the actual effects of the prestressed layer, four spherical transducers numbered from 1#–4# are fabricated, and the corresponding radial prestresses are listed in Table 4. As shown in Fig. 8, the resonance frequency (f_s) increases with the growth of the radial prestress (T_r). This variation is consistent with the experimental results of Arnold.[29,43] Thus, we could adopt a similar assumption that the radial prestress introduced by the prestressed layer improves the effective coupling of the piezoelectric ceramic and the sealing layer. As to the FEA model, the radial prestress is simulated with a boundary load, and the effective coupling is idealized as 100%, resulting in constant resonance frequency.

The TVR varies with the frequency, peaking at f_s. The $\mathrm{TVR}_{\mathrm{max}}$ reaches a peak value of 150.2 dB for 2# transducer with a 1.18 MPa T_r. The variation of $\mathrm{TVR}_{\mathrm{max}}$ on T_r is different from that in FEA because the FEA model ignores the prestressed layer where a great number of acoustic energies were reflected back and forth before reaching the water. As listed in Table 4, the average acoustic impedance (Z_{ave}) of the prestressed layer and the sealing layer grows with T_r for 1#–4# transducers. According to Eq. (12), the optimum acoustic impedance to realize the maximum transmitted energy is 4.29 Mrayls. Therefore, the increasing Z_{ave} could help mitigate the enormous impedance mismatch between the piezoelectric ceramic and water, achieving efficient energy transfer and greatly increasing the performance of transducer.[41,42] It should be noted that, however, attenuation increases with the growth of the interfaces in the prestressed layer.[42] According to Eq. (11), T_r increases linearly with the number of the fiber layer n. Hence, the number of interfaces grows with T_r, resulting in a peak $\mathrm{TVR}_{\mathrm{max}}$ with T_r.

Table 4. Summary of the average material and acoustic properties of the prestressed layer and the sealing layer.

No.	T_r (MPa)	n	h_p (mm)	h_S (mm)	ρ_{ave} (kg/m^3)	Z_{ave} (Mrayls)
1#	0	0	0.57	4.238	1087	1.7
2#	1.18	2	1.102	3.506	1150	1.9
3#	2.29	4	1.578	2.793	1221	2.2
4#	3.44	6	2.11	2.498	1291	2.3

The transmitting sound level (SL) is further tested under various voltages. SL shows an upward trend with T_r at 150 V and 200 V for all the four transducers, and for 3# and 4# transducers at 250 V. It is worth mentioning that when the drive voltage grows up to 250 V, 1# transducer (T_r = 0MPa) and 2# transducer (T_r = 1.18MPa) could not work normally. Further, the maximum transmitting sound level ($\mathrm{SL}_{\mathrm{max}}$) of the four transducers are measured through the increase of voltage. $\mathrm{SL}_{\mathrm{max}}$ grows steadily with T_r, showing a 3.9 dB ascend from 200.7 dB to 204.6dB. The variations of $\mathrm{SL}_{\mathrm{max}}$ on T_r and V_{rms} agree with those in FEA. Overall, the maximum drive voltage increases with T_r, resulting in noticeable ascend of $\mathrm{SL}_{\mathrm{max}}$. This is a strong credibility that the radial prestress could help improve the transmitting performances of the spherical transducer.

4. Conclusion

This paper involves a theoretical estimation of the radial stress on the outer radius of the hollow piezoelectric sphere for the geodesic filament winding strategy. The ideal effect of the radial prestress is analyzed with the assistance of FEA. The properties of the perestress layer and four spherical

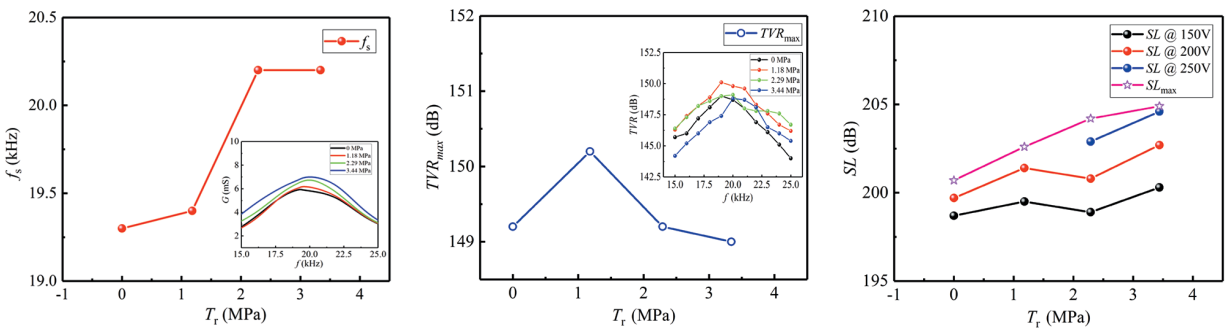

Fig. 8. Summary of experimental results of four spherical transducers measured in an anechoic pond, variation of (a) resonance frequency (f_s), (b) TVR, and (c) transmitting sound level (SL) with radial prestress and voltage.

transducers were tested experimentally. In summary, the following conclusions are obtained:

(1) The radial stress (T_r) on the outer radius of the hollow piezoelectric sphere could be estimated quantitatively with a thin shell approximation, and adjusted through the number of the fiber layer (n) and the tensile force (F).
(2) The acoustic impedance of the prestressed layer grows with T_r, and help mitigate the enormous impedance mismatch between the piezoelectric ceramic and water.
(3) FEA results show that the resonance frequency (f_s), the maximum transmitting voltage response (TVR_{max}), and the maximum transmitting sound level (SL_{max}) remains relatively stable with T_r. By contrast, SL_{max} jumps markedly with voltage, from 193.5 dB at 150 V to 199.5 dB at 300 V.
(4) The test results of four spherical transducers shows that f_s grows with T_r. The attenuation of the acoustic energy in prestressed layer leads to a peak value of TVR_{max} at 1.18 MPa. The maximum drive voltage increases with T_r, resulting in a steady growth of SL_{max}, with a noticeable ascend of 3.9 dB at a 3.44 MPa T_r.
(5) The results provide a good paradigm for the design of prestressed spherical transducers with high sound radiation performance.

Acknowledgments

This work was financially supported by the National Natural Science Foundation of China (Nos. U1806221 and U2006218), Shandong Provincial Natural Science Foundation (Grant No. ZR2020KA003), Taishan Scholars Program and case-by-case project for Top Outstanding Talents of Jinan, the Project of "20 Items of University" of Jinan (Grant Nos. T202009 and T201907).

References

[1]S. Hur, H. Choi, G. H. Yoon, N. W. Kim, D. G. Lee and Y. T. Kim, Planar ultrasonic transducer based on a metasurface piezoelectric ring array for subwavelength acoustic focusing in water, *Sci. Rep.* **12**, 1485 (2022), doi:10.1038/s41598-022-05547-7.
[2]T. E. Hooper, J. I. Roscow, A. Mathieson, H. Khanbareh, A. J. Goetzee-Barral and A. J. Bell, High voltage coefficient piezoelectric materials and their applications, *J. Eur. Ceram. Soc.* **41**, 6115 (2021), doi:10.1016/j.jeurceramsoc.2021.06.022.
[3]B. Y. Li, X. M. Chen, M. D. Liu, Z. D. Yu, H. L. Lian and J. P. Zhou, Improved ferroelectric and piezoelectric properties of $(Na_{0.5}K_{0.5})NbO_3$ ceramics via sintering in low oxygen partial pressure atmosphere and adding LiF, *J. Adv. Dielectr.* **11**, 2150012 (2021), doi:10.1142/S2010135X21500120.
[4]L. Chen, H. Liu, H. Qi and J. Chen, High-electromechanical performance for high-power piezoelectric applications: Fundamental, progress, and perspective, *Prog. Mater. Sci*. **127**, 100944 (2022), doi:10.1016/j.pmatsci.2022.100944.
[5]S. Sadeghpour, S. Meyers, J. P. Kruth, J. Vleugels and R. Puers, Single-element omnidirectional piezoelectric ultrasound transducer for under water communication, *Proc. Eurosensors* **1**, 363 (2017), doi:10.3390/proceedings1040363.
[6]J. George, D. D. Ebenezer and S. K. Bhattacharyya, Receiving sensitivity and transmitting voltage response of a fluid loaded spherical piezoelectric transducer with an elastic coating, *J. Acoust. Soc. Am.* **128**, 1712 (2010), doi:10.1121/1.3478776.
[7]G. Y. Karapetyan, V. E. Kaydashevy, M. E. Kutepov, T. A. Minasyan, V. A. Kalininz, V. O. Kislitsynz and E. M. Kaidashev, Tunable high-Q SAW resonator loaded on a changing capacitance, *J. Adv. Dielectr.* **10**, 2060009 (2020), doi:10.1142/S2010135X20600097.
[8]T. I. Belyankova, E. I. Vorovich, V. V. Kalinchuk and O. M. Tukodovaz, Peculiarities of surface acoustic waves, propagation in structures with functionally graded piezoelectric materials, coating from different ceramics on the basis of PZT, *J. Adv. Dielectr.* **10**, 2060017 (2020), doi:10.1142/S2010135X20600176.
[9]T. Naroliay, V. K. Guptay and I. A. Parinovz, Design and analysis of a shear mode piezoelectric energy harvester for rotational motion system, *J. Adv. Dielectr.* **10**, 2050008 (2020), doi:10.1142/S2010135X20500083.
[10]T. Jiang, B. He, Y. Zhang and L. Wang, Detecting of the longitudinal grouting quality in prestressed curved tendon duct using piezoceramic transducers, *Sensors* **20**, 1212 (2020), doi:10.3390/s20041212.
[11]C. G. Karayannis, C. E. Chalioris, G. M. Angeli, N. A. Papadopoulos, M. J. Favvata and C. P. Providakis, Experimental damage evaluation of reinforced concrete steel bars using piezoelectric sensors, *Constr. Build. Mater.* **105**, 227 (2016), doi:10.1016/j.conbuildmat.2015.12.019.
[12]Y. Gou and X. Fu, Vibration and horizontal directivity analysis of transmitting transducer for acoustic logging while drilling, *J. Geophys. Eng.* **18**(3), 379 (2021), doi:10.1093/jge/gxab021.
[13]Y. Geng, L. Xu, X. Li and L. Xu, Directivity analysis of piezoelectric micromachined ultrasonic transducer array, *Sens. Transducers* **111**, 45 (2009), https://www.researchgate.net/publication/281452525.
[14]Q. Huan, M. Chen, A. K. Soh and F. Li, Development of an omni-directional shear horizontal wave transducer based on a radially poled piezoelectric ring, *Acta Mech. Solida Sin.* **32**, 29 (2019), doi:10.1007/s10338-018-0059-x.
[15]S. Alkoy, R. J. Meyer, W. J. Hughes, J. K. Cochran Jr. and R. E. Newnham, Design, performance and modeling of piezoceramic hollow-sphere microprobe hydrophones, *Meas. Sci. Technol.* **20**, 095204 (2009), doi:10.1088/0957-0233/20/9/095204.
[16]H. Zhao, H. Li, Y. Wang, Z. Liu, J. Bian and T. Zhou, Design and implementation of half-space radiation high frequency broadband "spherical" transducer based on anti-sound baffle and circuit matching, *Appl. Acoust.* **188**, 108566 (2022), doi:10.1016/j.apacoust.2021.108566.
[17]J. O. Kim, J. G. Lee and Y. C. Han, Radial vibration characteristics of spherical piezoelectric transducers, *Ultrasonics* **43**, 531 (2005), doi:10.1016/j.ultras.2005.01.004.
[18]I. A. Loza and N. A. Shul'ga, Axisymmetric vibrations of a hollow piezoceramic sphere with radial polarization, *Sov. Appl. Mech*. **20**, 113 (1984). https://doi.org/10.1007/BF00883933.
[19]J. L. Butler, K. D. Rolt and F. A. Tito, Piezoelectric ceramic mechanical and electrical stress study, *J. Acoust. Soc. Am.* **96**, 1914 (1994), doi:10.1121/1.410205.
[20]A. Meshkinzar and A. M. Al-Jumaily, Vibration and acoustic radiation characteristics of cylindrical piezoelectric transducers with circumferential steps, *J. Sound Vib.* **511**, 116346 (2021), doi:10.1016/j.jsv.2021.116346.
[21]H. Li, Z. D. Deng, Y. Yuan and T. J. Carlson, Design parameters of a miniaturized piezoelectric underwater acoustic transmitter, *Sensors* **12**, 9098 (2012), doi:10.3390/s120709098.
[22]T. Fett, D. Munz and G. Thun, Tensile and bending strength of piezoelectric ceramics, *J. Mater. Sci. Lett.* **18**, 189 (1999), doi:10.1023/A:1006698724548.

[23]K. Adachi, I. Ogasawara, Y. Tamura, M. Makino and N. Kato, "Influence of static prestress on the characteristics of bolt-clamped Langevin-type transducers, *Jpn. J. Appl. Phys.* **37**, 2982 (1998), doi:10.1143/JJAP.37.2982.
[24]B. Fu, T. Li and Y. Xie, Model-based diagnosis for pre-stress of langevin transducers, *2009 IEEE Circ. Syst. Int. Conf.* (2009), pp. 1–4, (Chengdu, China), doi:10.1109/CAS-ICTD.2009.4960840.
[25]F. T. Calkins, M. J. Dapino and A. B. Flatau, Effect of prestress on the dynamic performace of a Terfenol-D transducer, *Proc. SPIE Int. Soc. Opt. Eng., Proc. SPIE Smart. Struct. Mater.* **23**, 3041 (1997), doi:10.1117/12.275654.
[26]T. I. Belyankova, E. I. Vorovich, V. V. Kalinchuk and O. M. Tukodovaz, Specific features of SH-waves propagation in structures with prestressed inhomogeneous coating made of piezoceramics based on LiNbO3, *J. Adv. Dielectr.* **11**, 2160007 (2021), doi:10.1142/S2010135X21600079.
[27]D. Audigier, Cl. Richard, Cl. Descamps, M. Troccaz and L. Eyraud, PZT uniaxial stress dependence: Experimental results, *Ferroelectrics* **154**, 219 (1994), doi:10.1080/00150199408017289.
[28]H. H. A. Krueger and D. Berlincourt, Effects of high static stress on the piezoelectric properties of transducer materials, *J. Acoust. Soc. Am.* **33**, 1339 (1961), doi:10.1121/1.1908435.
[29]F. J. Arnold and S. S. Mühlen, The resonance frequencies on mechanically pre-stressed ultrasonic piezotransducers, *Ultrasonics* **39**, 1 (2001), doi:10.1016/S0041-624X(00)00047-0.
[30]X. Peng, L. Hu, W. Liu and X. Fu, Model-based analysis and regulating approach of air-coupled transducers with spurious resonance, *Sensors* **20**, 6184 (2020), doi:10.3390/s20216184.
[31]M. J. Dapino, A. B. Flatau and F. T. Calkins, Statistical analysis of terfenol-d material properties, *J. Intell. Mater. Syst. Struct.* **17**, 587 (2006), doi:10.1177/1045389X06059500.
[32]B. Thompson and H. S. Yoon, A prestress measurement circuit for piezoceramic stack transducers, *IEEE Sens. J.* **11**, 2349 (2011), doi:10.1109/JSEN.2011.2123882.
[33]H. Fang, Y. Liu, T. Zhao, Y. Liu, K. Li, D. Sun and D. Zhang, Design of a flextensional transducer with adjustable prestress, *J. Phys.*: *Conf. Ser*. **2012**, 012017 (2021), doi:10.1088/1742-6596/2012/1/012017.
[34]J. Xu, S. Lin and J. Hu, Electromechanical equivalent circuit and coupled vibration of the radially composite cylindrical piezoelectric transducer, *Sens. Actuator A Phys.* **286**, 113 (2019), doi:10.1016/j.sna.2018.12.023.
[35]S. Lin, Study on the radial composite piezoelectric ceramic transducer in radial vibration, *Ultrasonics* **46**, 51 (2007), doi:10.1016/j.ultras.2006.10.005.
[36]X. F. Zhang, X. J. lin, C. H. Yang, X. Cheng and S. F. Huang, Effects of radial pressure on piezoelectric ceramic tubes and transducers, *J. Acoust. Soc. Am.* **151**, 434 (2022), doi:10.1121/10.0009319.
[37]M. Rong and B. Liu, Fiber trajectories design of ellipsoid component based on topological mapping methodology, *Appl. Compos. Mater.* **24**, 661 (2017), doi:10.1007/s10443-016-9533-0.
[38]S. Alkoy, A. Dogan, A. C. Hladky, P. Langlet, J. K. Cochran and R. E. Newnham, Miniature piezoelectric hollow sphere transducers, *Proc. IEEE Int. Freq. Contr. Symp.* (1996), pp. 586–594, (Honolulu, HI, USA), doi:10.1109/FREQ.1996.559930.
[39]S. Timoshenko and J. N.Goodier, *Theory of Elasticity*, (McGraw Hill Book Company, New York, 1951), pp. 356–359.
[40]C. S. Desilets, J. D. Fraser and G. S. Kino, The design of efficient broad-band piezoelectric transducers, *IEEE Trans. Son. Ultrason.* **25**, 115 (1978), doi:10.1109/T-SU.1978.31001.
[41]C. Wong, S. Chan, W. C. Wu, C. Suen, H. Yau, D. Y. Wang, S. Li and J. Y. Dai, Tunable high acoustic impedance alumina epoxy composite matching for high frequency ultrasound transducer, *Ultrasonics* **116**, 106506 (2021), doi:10.1016/j.ultras.2021.106506.
[42]V. T. Rathod, A review of acoustic impedance matching techniques for piezoelectric sensors and transducers, *Sensors* **20**, 4051 (2020), doi:10.3390/s20144051.
[43]F. J. Arnold and S. S. Mühlen, The mechanical pre-stressing in ultrasonic piezotransducers, *Ultrasonics* **39**, 7 (2001), doi:10.1016/S0041-624X(00)00048-2.